

## The Atmospheric Infrared Sounder on EOS

H. H. Aumann and R. Pagano  
Jet Propulsion Laboratory  
California Institute of Technology  
Pasadena, California 91109

Recent breakthroughs in infrared detector array and cryocooler technology have made it possible to convert the concepts of optimum, passive, infrared sounding to a practical satellite-borne instrument: the Atmospheric Infrared Sounder (AIRS), a grating array infrared spectrometer temperature sounder. AIRS, together with the Advanced Microwave Sounding Unit (AMSU) and the Microwave Humidity Sounder (MHS), will form a complementary sounding system for the Earth Observing Systems (EOS), to be launched in the year 2000. The three instruments are expected to become the new operational sounding system for the National Oceanic and Atmospheric Administration (NOAA).

### 1. Introduction

AIRS is a high-spectral-resolution infrared spectrometer which, together with the AMSU and the MHS microwave sounders, is designed to meet NASA's global change research objectives and NOAA's operational weather prediction requirements. The NOAA Numerical Weather Service (NWS) has repeatedly stated that more accurate global temperature and moisture profiles will be required than are presently available to improve short-range (up to 3 days) and medium-range (up to 10 days) weather forecasts. Specifically, the NWS requires temperature profiles with 1°C accuracy in 1-km thick layers and humidity profiles with 20 percent accuracy in the troposphere. The objective of AIRS is to provide these improved global temperature and moisture profiles. The NOAA specifications are based on numerical modeling; however, an intuitive argument leads to the same conclusion: the sounding accuracy currently obtained from the radiosonde network covering the continental United States

is approximately 1°C, while the accuracy of the soundings from space observations over oceans is limited by the current NOAA operational infrared and microwave sounders, the High Resolution Infrared Sounder (HIRS/2) and the Microwave Sounding Unit (MSU), to about 2.5°C in 2-km thick layers. As a result, the 1°C accuracy available over land tends to give good short-range forecasts over the continent, provided that the effects of ocean circulation do not dominate the land effects. However, this condition is seldom satisfied on a time scale of more than a day. Consequently, even NOAA's short-range forecast skill is significantly degraded. The availability of 1°C accuracy over the entire globe is thus key to achieving accurate short- and medium-range forecasts.

The basic physics involved in the design of a temperature sounder from Earth orbit was published in the late 1950's (Kaplan 1959). Ten years later, and shortly after Chahine (1968) published the relaxation algorithm to invert spectral radiances to temperature profiles, the first experimental temperature soundings from space were achieved using the Satellite Infrared Radiation Spectrometer (SIRS). SIRS was a seven-channel grating spectrometer with a resolution ( $\lambda/\Delta\lambda$ ) of 100 in the 15- $\mu\text{m}$  CO<sub>2</sub> band on Nimbus-4 (Wark and Hilleary 1969). The first infrared temperature sounders required a cloud-free field of view, a condition which is seldom satisfied. Smith (1968) proposed the N\* parameter for "cloud-clearing". Clouds become optically thick much quicker in the infrared (15 $\mu\text{m}$  = 0.015 cm) than at 57-GHz (0.5-cm) microwave sounding frequencies. Staelin et al. (1973) demonstrated the capability to sense atmospheric temperatures within and below clouds in the microwave region with the Nimbus-E Microwave Sounder (NEMS). Unfortunately, the vertical resolution achievable in the troposphere from the microwave region is inferior to that achievable in the 4.3- $\mu\text{m}$  CO<sub>2</sub> band. In 1974 Chahine proposed a physical basis for cloud-clearing infrared radiances and Smith et al. demonstrated the N\* technique using the Infrared Temperature Profile Radiometer (ITPR) on the Nimbus-5 satellite. Aumann and Chahine (1976) and M. T. Chahine, H. H. Aumann, and F. W. Taylor (1977) demonstrated temperature sounding of partly cloudy atmospheres using 4.3- $\mu\text{m}$  CO<sub>2</sub> and 11- $\mu\text{m}$  window channels. A cloud-clearing technique, which combines the use of infrared and microwave data, is now routinely applied in the NOAA

operational sounding system. This method takes advantage of the fact that, to first order, the microwave data are not affected by clouds. It makes the assumption that the horizontal inhomogeneity in the scene due to clouds is much larger than the inhomogeneity due to temperature profile changes on the scale of a microwave field of view. By 1978 the HIRS-2, a radiometer with spectral resolution of about 75, with 19 channels between 3.7 and 15  $\mu\text{m}$ , and the MSU (a follow-up to NEMS) with four channels near the 57-GHz oxygen band became the first of the Topographical Infrared Operations Satellites (TIROS) Operational Vertical Sounders (TOVS). These two instruments still constitute the current operational NOAA sounding system.

The limitation of the performance of the TOVS sounders lies in the limitations of infrared technology of the early seventies: spectral resolution was limited to two percent of the wavelength by discrete interference filters, detector technology limited a sounder to a few discrete detectors, and passive radiators precluded detector temperatures below 90K. Kaplan et al. (1977) showed that a major improvement in vertical resolution and accuracy could be achieved by increasing the spectral resolution to 1200 and by using many more sounding channels, including the R-branch of the 4.2- $\mu\text{m}$   $\text{CO}_2$  band. It took another ten years, until the late 1980's, before the following infrared technology breakthroughs occurred that made it possible to incorporate this knowledge into a practical instrument, AIRS:

- (1) Array technology in HgCdTe detectors makes it possible to provide contiguous coverage of most of the 3.7- to 15.4- $\mu\text{m}$  region of the spectrum with over 2000 detectors.
- (2) The technology of active refrigerators improved dramatically in the areas of efficiency and reliability. This makes it possible to operate the detectors at a temperature of 60 K, instead of 90 K. This is particularly important near 15  $\mu\text{m}$ , where it results in a very large increase in detector performance.
- (3) The combination of miniature infrared filters and integrated circuit readout devices allows the small focal plane dimension to be efficiently coupled to a classical grating and spatial scanning device.
- (4) The hundred-fold increase in the number of channels of AIRS

compared to HIRS results in a proportional increase in the computational complexity for the ground data system. The inversion of a radiance spectra to temperature and moisture profiles is computationally intensive. The large gain in computer power over the last decade makes it feasible to handle the much larger number of channels with confidence.

In this paper we describe the AIRS instrument, with particular emphasis on the electro-optical technology that made the breakthrough in sounder performance possible.

## 2. AIRS Experiment Description

Achievement of the major breakthrough in sounding accuracy requires coverage of sounding regions over a wide part of the key areas of the electromagnetic spectrum, high spectral resolution, accurate spectral and radiometric calibration, and a high signal-to-noise ratio. The AIRS experiment utilizes the data from three instruments on the EOS platform: AIRS (which will be described in more detail in the following section), AMSU, and MHS. The AIRS instrument sounds the temperature profile in the 4.3- $\mu\text{m}$  and 15- $\mu\text{m}$   $\text{CO}_2$  band. It sounds the water vapor profile in the 6- $\mu\text{m}$  water band. The AMSU is an advanced version of the MSU. Its purpose is to allow AIRS temperature retrievals under partially cloudy conditions. AMSU-A is a 15-channel microwave radiometer with channels between 23.8 and 89.0 GHz. Eight of these channels sound the atmospheric temperature in the 57-GHz oxygen band. The AMSU footprint diameter is three times larger than the AIRS footprint. The AIRS scan pattern and the superimposed AMSU footprints are shown in Fig. 1. For each AMSU footprint there are nine AIRS footprints, to permit effective cloud-clearing. In addition there are nine MHS footprints which overlay the AIRS footprints. The MHS has six channels, five in the 183-GHz water band. These channels are sensitive to water vapor and to the liquid droplet content of the atmosphere, while the AIRS channels in the 6.3- $\mu\text{m}$  water band are sensitive only to water vapor. The ground-based data processing system combines the data from AMSU, AIRS, and MHS to produce one temperature and moisture sounding for each AMSU footprint.

### 3. AIRS Instrument Requirements

The measurement requirements for AIRS were established by an Interagency Sounder Team. They are documented in the AIRS Functional Requirements Document (JPL D-8236). The highest level requirements are summarized in Table 1. Since the requirements deal with the information content of the spectrum, that is, spectral coverage, spectral resolution, and the signal-to-noise ratio, they are independent of detailed instrument implementation. With more than 2400 spectral resolution elements required to cover the 3.7- $\mu\text{m}$  to 15.4- $\mu\text{m}$  region of the spectrum, only two implementation concepts can be envisioned: a grating array spectrometer or a Michelson interferometer. If the required wavelength region can be covered with background photon-noise-limited detector arrays, the grating array spectrometer outperforms the Michelson interferometer (see appendix). In the early eighties, such arrays did not exist. However, as part of the Strategic Defense Initiative (SDI) effort, major advances were achieved in the development of detector arrays for the thermal infrared and in the cooling power, efficiency, and lifetime of active coolers necessary to operate the detectors at 60 K. In 1987 NASA made the decision to implement AIRS as a grating array spectrometer and to support the AIRS design-specific detector and cooler technology development. The anticipated advances in detector array and cryocooler technology have since been achieved (Krueger et al. 1993, Kotsubo et al 1992).

### 4. AIRS Instrument Description Overview

The AIRS Instrument is a pupil-imaging, multi-aperture, echelle grating spectrometer, providing coverage of the infrared spectral regions as listed in Table 1. A single, low-spectral order spectrometer provides a (nominal) resolution,  $\lambda/\Delta\lambda$ , of 1200 between 3.7- $\mu\text{m}$  and 15.4- $\mu\text{m}$ . The scan pattern is shown in Fig. 1. Every 2.67 sec, AIRS scans a  $\pm 49.5$  deg swath around nadir in a direction perpendicular to the EOS satellite's ground track. Each scan line contains 90 ground footprints, a hot calibration view, a space calibration view, and a spectral calibration view. The instantaneous field of view (IFOV) of the AIRS infrared (IR) spectrometer is 1.1 deg, providing a 13.5-km ground footprint at nadir from a 705-km orbital altitude. AIRS

obtains one spectrum for every footprint in 0.022 sec. In addition to the IR grating spectrometer, the AIRS instrument contains a four-color, visible and near infrared (VIS/NIR) photometer with a 0.185-deg IFOV. The spectral bandwidth of the VIS/NIR channels is defined by bandpass filters and covers the spectral wavelengths from 400 to 1000 nm. The footprint of the VIS/NIR channels will be spatially coregistered with the IR footprint and will provide contiguous ground coverage at all scan angles. The purpose of these channels is to aid in the discrimination between low-level clouds and snow and to allow empirical coregistration of the AIRS infrared channels with other instruments on EOS, in particular the Moderate Resolution Infrared Spectrometer (MODIS).

#### 4.1 Functional Description

Figure 2 shows an X-ray view of the AIRS instrument. At the top level, the AIRS instrument consists of a mechanical structure, a scan mirror assembly, a VIS/NIR assembly, an IR spectrometer, an IR focal plane/dewar assembly, an electronics assembly, and a cryogenic thermal control system. Sets of bench checkout equipment (BCE) and ground support equipment (GSE) assist the testing and ground operation of the AIRS instrument. The support structure of the optical component, shown in Fig. 2, is the interface for many of the major subassemblies and provides a stable mounting configuration under launch and on-orbit dynamics. The scan mirror assembly, including radiometric and spectral calibrators, is mounted to the support structure via an independent truss support and will be aligned to the spectrometer. The heat generated in this assembly will be conductively linked to a cold plate. The IR spectrometer interfaces to its support truss via kinematic mounts. These mounts will be designed to support the IR spectrometer about its center of gravity. They will allow the IR spectrometer to dimensionally change without inducing stresses into the optical housing or mirrors. A two-stage radiator is conductively linked to the IR spectrometer housing and cools it to 155 K.

#### 4.2. The IR Spectrometer

A conceptual schematic of the IR spectrometer is shown in Fig. 3. The

spectrometer images the entrance pupil onto the array of detectors. The pupil-imaging method was chosen to avoid measurement errors due to detector non-uniformities in the presence of a high contrast scene. Spectral dispersion is accomplished by an echelle diffraction grating. This type of dispersing element utilizes overlapping grating orders to provide wide spectral coverage over moderate diffraction angles. The traditional approach to spectral order separation is to use a second dispersing element which is oriented orthogonally. However, the crossed gratings cause lower optical efficiency, increased grating scatter, and non-parallel spectral orders at the focal plane. The AIRS spectrometer design uses a multi-aperture approach to separate spectral orders. The telescope entrance pupil is subdivided into several apertures. A bandpass filter is used with each aperture to select the spectral order of interest and to reject out-of-band radiation. The multi-aperture design approach allows the area of each aperture to be individually adjusted to provide the required signal-to-noise ratio. This design also provides the focal plane flexibility that is essential to achieving a producible system. In order to achieve the optical wavefront error (WFE) stability requirements, the optics and housing of the spectrometer will be manufactured using the same material to produce an athermalized system. Aluminum has been selected because of its physical properties that allow diamond-turning of both mirrors and optical mounts, as well as shaping of diffraction gratings. Openings in the ribbed walls of the spectrometer housing, in conjunction with diamond-machined pads and precision pins, will provide mirror alignment. The goal is to machine-in the alignment and minimize the adjustments.

An optical schematic of the IR spectrometer is shown in Fig. 4. Incoming radiation is reflected by a scan mirror to a series of entrance apertures. Individual afocal relay telescopes demagnify the apertures and create spaces that are needed between detector arrays at the focal plane. A telescope provides a ground image at the field stop, which is relayed to the grating by a pair of confocal parabolas. The dispersing element is an echelle grating (12 lines/mm) with a superimposed aspheric profile to correct the wavefront error of the Schmidt camera. A nominal diffracted angle of zero degrees was chosen to minimize the diffracted field of view and to satisfy the symmetry condition for Schmidt correction. The Schmidt design was

chosen because of the large spectral bandpass, low f-number capability (the AIRS design is  $f/1.7$ ), and moderate field-of-view requirements. A field-flattening lens is used close to the focal plane to correct the field curvature of the Schmidt camera. The Schmidt camera interfaces to the main housing, using a low expansion material. This controls the amount of optical shift over the allowable temperature variations of the spectrometer. A passive athermal design approach is employed to maintain performance over all environments anticipated. As a fail-safe device, an alignment adjustment mechanism is incorporated to adjust both the tilt and focus of the spectrometer camera over a limited range. The focal plane consists of rows of detectors which correspond to the dispersed image of each entrance aperture. The relationship between the entrance pupil map and the focal plane color map is shown in Fig. 5.

In the multi-aperture system, each linear array is illuminated by several overlapping spectral orders. Bandpass filters are used to select the spectral order of interest for each linear array. To block the unwanted radiation entering the spectrometer telescope, a filter is located over each entrance aperture. A second filter is placed over each linear array. This two-stage-series filter approach is necessary for two reasons. First, the bandpass filters over the entrance apertures minimize stray light within the optical system, while the focal plane filters suppress thermally emitted radiation from the optical elements and the structure. Second, the demanding blocking requirements placed on the filters necessitate a two-stage approach. To accomplish this, the entrance aperture roughly defines the bandpass and rejects wavelengths farther from the bandpass center, while the focal plane filter defines the steep edge slopes and rejects wavelengths just beyond the spectral region of interest.

By far the more challenging set of filters is the focal plane set. Each of the 27 multilayer focal plane filters is approximately 0.4-mm wide by 10-mm long and separated from the next adjacent filter by only 0.5 mm. Filter thicknesses must be accurately matched to meet the optical performance requirements. The filters will be manufactured with two to three filters per substrate. The substrates will be assembled in an electroformed frame which, in turn, attaches to strategic locations on the focal plane. Opaque baffles are deposited onto the surface of the filter assembly to limit

stray light and crosstalk.

The spectral response function is dominated by the convolution of the spectrometer entrance slit, the optics point spread function, and the detector aperture (the spectrometer exit slit), but also includes the effects of scatter and ghost images. The requirement is that 50 percent of the integrated spectral response function shall be within one resolution element and 95 percent within two resolution elements. The 95 percent criteria is met with an optical wavefront error of 1/10 wave at 10.6  $\mu\text{m}$ . The optical tolerances are not tight, except for those that affect the final f/1.7 focus, such as the filter thickness match, Schmidt camera alignment, and the detector position.

#### 4.3 IR Focal Plane/Dewar Assembly

The overall focal plane requirements have been derived based on a marriage between system requirements and projected focal plane capabilities. The key requirements are listed in Table 2.

The baseline IR detector/dewar assembly meeting these requirements is shown in Fig. 6. The assembly consists of a single vacuum dewar with the focal plane shown in Fig. 5. The focal plane uses 15 linear arrays of HgCdTe detectors, each with up to 250 elements. The AIRS requirement for these linear arrays was the driving force in advancing the state of the art for moderately cooled linear arrays of HgCdTe detectors in the 3.7- to 15.4- $\mu\text{m}$  region. Between 4 and 13.6  $\mu\text{m}$ , the detectors operate in the photovoltaic mode and are photon noise limited. Beyond 13.6  $\mu\text{m}$ , the detectors operate in the photoconductive mode and are  $R_0A$  detector noise limited. The photovoltaic detectors are mounted to silicon signal processor assemblies which collect the signals from the detectors; perform first-level signal processing, such as band limiting; and multiplex the signals to a few outputs. The photoconductive detectors have an output line for each detector. Spectral filters are mounted in an assembly above the focal plane to assist in spectral definition.

The focal plane architecture is driven by the requirements for an efficient optical configuration, the area required for low noise signal multiplexing, the location of detectors to avoid spectral gaps, and the design for minimum module diversity, spacing, and alignment complexity. The linear detector arrays are distributed among

12 modules, one containing photoconductive detectors with individual wires out for each element and 11 containing photovoltaic detectors mounted to multiplexers. Each module consists of detectors and multiplexers (for PV detectors). Individual photovoltaic detector arrays are arranged in a bilinear format. There are two independent detectors per spectral sample with independent multiplexers so that failure of a detector or even an entire multiplexer will not lead to the complete loss of information. There is not room nor lead capability for detector redundancy for the longest spectral bands covered by photoconductive detectors; however, even there, signal and return lines are partitioned to avoid complete loss of information from interconnect losses.

The design of the focal plane readout is strongly interrelated with the detector layout and the integrated circuit process capability. A key driver is the available area on the silicon to support the required functions. The modules are fabricated and tested individually, and then mounted with shims on the focal plane substrate to improve assembly yield. Note that the focal plane has a resolution element count of 1218; the required Nyquist sampling doubles the minimum detector count to 2436. Including component redundancy, the AIRS focal plane contains 4456 active elements in the space of only 8.2 by 36.9 mm.

The key requirement for the cryosystem is to provide a 60 K, or lower, detector temperature with a five-year, or longer, operating life. The cryosystem heat load consists of several components, including detector bias, lead wire conduction, support conduction, and radiative losses. The predicted cooler heat load is 0.92 W. The cooler power input was calculated utilizing the data measured during the cooler development program and allowing for an end-of-life temperature degradation of 5 K. The required cooler power input is 82 W with a beginning-of-life refrigeration capacity of 1.25 W at 55 K. The refrigeration capacity is required to provide a margin for both thermal and cooler degradation with time.

To achieve the required cooler performance, several split-Stirling cooler designs were developed and tested during the cooler technology program. The objective of the program was to develop a cooler capable of meeting the AIRS requirements for refrigeration capacity and efficiency. The approach adopted was to

expand the present cooler performance, while still maintaining the design heritage of the Oxford-type coolers developed for the Integrated Switching And Multiplexing Sounders (ISAMS) and the Along Track Scanning Radiometer (ATSR). This design heritage was based on a direct current (DC) powered linear split-cycle Stirling refrigerator with clearance seals and flexure-supported pistons. The increased performance was found to be associated with larger volumetric flow rates achievable with increased compressor size. The prototype cooler exceeded the AIRS requirement, by achieving 1.3 W of cooling at 52 K with 55 W of compressor power.

#### 4.4. System Sensitivity

The AIRS instrument has been modeled to ascertain its level of performance under minimum, nominal, and maximum scene conditions. The predicted sensitivity of the AIRS Instrument is plotted as a function of the waveband in Fig. 7. The results indicate that noise equivalent delta temperature (NEDT) requirements can be met at all AIRS wavelengths. To accommodate unmodeled noise factors, fabrication tolerancing, and statistical variations in the performance of individual spectral channels, a sensitivity margin factor of two is highly desirable. This margin is generally achieved over the wavelength range from 4 to 12  $\mu\text{m}$ . There is little margin in atmospheric window channels below 4  $\mu\text{m}$ , where the limiting factors are multiplexer  $1/f$  noise and scene BLIP conditions. In the 12- to 13.6- $\mu\text{m}$  region, the NEDT increases from 0.10 K to 0.14 K due to noise effects related to the decreasing value of the  $R_0A$  product in the PV:HgCdTe detector arrays. Beyond 13.6  $\mu\text{m}$ , PC:HgCdTe detector arrays are used. The photoconductive detectors require chopping at 405 Hz to remove  $1/f$  noise, but still provide NEDT's in the range of 0.21 K to 0.26 K.

## 5. Conclusions

Recent breakthroughs in infrared detector array and cryocooler technology have made it possible to convert the concepts of optimum passive infrared sounding to a practical satellite-borne instrument: AIRS, a grating array infrared spectrometer temperature sounder. AIRS, together with the AMSU and MHS, will form a

complementary sounding system for EOS, to be launched in the year 2000. The three instruments are expected to become the new operational sounding system for NOAA.

#### Acknowledgments

Dr. David Wark, NOAA/National Environmental Satellite, Data, and Information Service (NESDIS), provided valuable clarifications regarding the early history of satellite-based temperature sounders. The AIRS instrument is being designed and built at LORAL/LIRIS in Lexington, Massachusetts under contract with the Jet Propulsion Laboratory. The technical description of AIRS (Section 3) and the figures used in this paper are based on the AIRS Experiment Implementation Plan, dated March 1, 1993, and generated with the assistance of the AIRS team at LORAL/LIRIS. The Jet Propulsion Laboratory, California Institute of Technology, operates under contract with the National Aeronautics and Space Administration.

#### References

- L. D. Kaplan, "Inferences of atmospheric structures from satellite remote radiation measurements," *J. Opt. Soc. Am.*, Vol. 49, pp 1004-1004 (1959).
- M. T. Chahine, "Determination of the temperature profile in the atmosphere from its outgoing radiance," *J. Opt. Soc. Am.*, Vol 58, pp 1634-1637 (1968).
- W. L. Smith, "An improved method for calculating tropospheric temperature and moisture from satellite radiance measurements," *Monthly Weather Review*, Vol. 96, pp 387-396 (1968).
- D. Q. Wark and D.T. Hilleary, "Atmospheric Temperature: A successful test of remote probing," *Science*, Vol. 165, pp 1256-1258 (1969).
- D. H. Staelin, A. H. Barrett, J. W. Waters, F. T. Barath, E. J. Johnston, P. W. Rosenkranz, N. E. Gant, and W. B. Lenoir, "Microwave spectrometer on the Nimbus-5 satellite: Meteorological and geophysical data," *Science*, Vol. 182, pp 1339-1339 (1973).
- M. T. Chahine, "Remote Sounding of Cloudy Atmospheres. I. The Single Layer Cloud," *J. Atm. Science*, Vol. 31, pp 700 - 700 (1974).
- W. L. Smith, D. T. Hilleary, J. C. Fischer, H. B. Howell, and H. M. Woolf, "The

- Nimbus-5 ITPR experiment," *Appl. Opt.*, Vol. 13, pp 449 - 449 (1974).
- H. H. Aumann and M. T. Chahine, "Infrared Multidetector Spectrometer for Remote Sensing of Temperature Profiles in the Presence of Clouds," *App. Opt.*, Vol.15, pp 2091-2091 (1976).
- M. T. Chahine, H. H. Aumann, and F.W. Taylor, "Remote Sounding of Cloudy Atmospheres. III. Experimental Verification," *J. Atm. Science*, Vol. 34, pp 758-758 (1977).
- L. D. Kaplan, M. T. Chahine, J. Susskind, and L. E. Searle, "Spectral band passes for a high precision satellite sounder," *Appl. Opt.*, Vol. 16, pp 322-325 (1977).
- E. E. Krueger, G. N. Pultz, K. R. Maschhoff, S. P. Tobin, P. W. Norton, J. H. Rutter and M. B. Reine, "Extending the HgCdTe Photovoltaic Detector Technology to cutoff wavelengths of 17- $\mu\text{m}$ ", *1993 Spring Meeting of the Materials Research Society, San Francisco, California, April 14-16, 1993*, to be published in Volume 299 of the proceedings series.
- V. Y. Kotsubo, D. L. Johnson, and R. G. Ross, "Calorimetric Thermal-Vacuum Performance Characterization of the BAe 80K Space Cryocooler", *SAE Paper No. 929037, Proceedings of the 27th Intersociety Energy Conversion Engineering Conference, San Diego, California, August 3-7, 1992*, P-259, Vol.5, pp 5.101-5.107.
- "AIRS Functional Requirements Document," JPL internal document D-8236, Rev.1. (October 1992).

## Appendix

### Comparison of Fourier Transform and Grating Array Spectrometers

In the early sixties, infrared spectroscopists utilized Fourier Transform spectrometers because of the multiplex advantage, compared to a grating spectrometer. If both spectrometers use a single, suitably cooled detector and the detector performance is not background noise limited, the multiplex advantage gains

in the signal-to-noise ratio (SNR) for a given total observation time by the square root of the number of resolution elements. For example, the Atmospheric Trace Molecule Spectrometer (ATMOS) is a Fourier spectrometer on the Space Shuttle. It takes spectra of the Sun from 500 to 4000  $\text{cm}^{-1}$  with a resolution of 0.01  $\text{cm}^{-1}$ . Since the spectrum contains 250,000 resolution elements, the multiplex gain is very large. A grating spectrometer would also enjoy the multiplex advantage if a separate detector were used for every spectral resolution element; that is, the entrance slit of the grating spectrometer is imaged onto a linear array. This concept becomes attractive if the instrument functional requirements can be satisfied with of the order of several thousand resolution elements, as in the case of AIRS, rather than over 100,000 elements, as in the case of the ATMOS experiment. In the following, we compare the relative SNR achievable per spectral element using a Fourier spectrometer (FS) and a grating array spectrometer (GA). We assume that

- (1) The FS uses one detector, while the GA employs an array for N detectors.
- (2) The detectors for both instruments are operating at the same temperature (in the 60 K vicinity).
- (3) Optics for both instruments are cooled (passively) to 100 K to 150 K to decrease the photon background.
- (4) The total time available to take one spectrum is the same. For AIRS at 705-km altitude, 0.022 seconds is available to obtain one spectrum and the required global coverage.
- (5) The detector area solid angle product ( $A*\Omega$ ) is the same for both instruments.

#### Definitions

- |       |   |
|-------|---|
| $S_n$ | Signal per spectral element                           |
| $B_n$ | Background flux per spectral element                  |
| $N$   | Number of contiguous spectral elements to be measured |
| $T$   | Total time available per spectrum                     |
| $N_d$ | Detector excess noise above photon noise              |

The spectral coverage requirements of the AIRS, as outlined in Table 1, and limitations on the performance of current HgCdTe arrays require us to distinguish three cases, depending on the type of noise which dominates: scene photon flux, background photon flux, or detector excess noise. In each case, we can express the SNR achievable with the grating array spectrometer,  $SNR_{ga}$ , in terms of the SNR achievable with a Fourier spectrometer,  $SNR_{ft}$ .

Case 1. In the 4- to 7- $\mu\text{m}$  region, the photon noise from the scene dominates.

$$SNR_{ft} = \frac{\sqrt{(S_n * T)}}{\sqrt{N}}$$

$$SNR_{ga} = \sqrt{N} * SNR_{ft}$$

$$SNR_{ga} = \sqrt{(S_n * T)}$$

Case 2. In the 7- to 12- $\mu\text{m}$  region, the photon flux from the instrument, that is, the background, is the dominant noise.

$$SNR_{ft} = \frac{S_n * \sqrt{T}}{\sqrt{(N * B_n)}}$$

$$SNR_{ga} = \sqrt{N} * SNR_{ft}$$

$$SNR_{ga} = \frac{S_n * \sqrt{T}}{\sqrt{B_n}}$$

Case 3. In the 3.7-to 4- $\mu\text{m}$  region and the 12- to 15.4- $\mu\text{m}$  region, the instrument performance is detector noise limited.

$$SNR_{ft} = SNR_{ga} = \frac{S_n * \sqrt{T}}{N_d}$$

In cases 1 and 2, the Fourier spectrometer suffers from the multiplex disadvantage: its SNR is lower than that of the grating array spectrometer by  $\sqrt{N}$ . In the case of the Fourier spectrometer, the photon noise originates from the entire spectral passband of the instrument, while the detectors of the grating spectrometer see only photons from the background in the narrow spectral resolution element of interest. In case 3, the Fourier spectrometer and the grating array spectrometer both enjoy the multiplex advantage.

The AIRS focal plane (Fig. 5) consists of 15 HgCdTe arrays, each optimized for its own particular wavelength region, with a total of 4456 active elements. If we assume that the interferometer uses three detectors, optimized for the short, middle, and far-infrared regions of the required spectral coverage, we can obtain an order of magnitude estimate of the multiplex disadvantage using  $\sqrt{N} = \sqrt{4456/3} = 38$ .

The Fourier spectrometer holds a big multiplex advantage over a single detector grating spectrometer; however, it suffers from the multiplex disadvantage when compare to a grating array spectrometer under photon noise limited conditions. Fourier spectrometer designs for temperature sounding from the EOS orbital altitude have been proposed which attempt to offset this disadvantage by using 3 by 3 detector area arrays. Use of area arrays increases the dwell time available per spectrum, in this case by a factor of nine and improves the signal-to-noise ratio by a factor of three. This reduces the multiplex disadvantage, but does not eliminate it. Excessive self-apodization prevents the use of larger spatial arrays at the AIRS required spectral resolution.

Table 1. AIRS High-Level Measurement Requirements

---

Spectral Coverage	3.74 to 4.61 $\mu\text{m}$ (2169 $\text{cm}^{-1}$ to 2674 $\text{cm}^{-1}$ )
$\lambda$	6.20 to 8.22 $\mu\text{m}$ (1265 $\text{cm}^{-1}$ to 1629 $\text{cm}^{-1}$ ) 8.80 to 15.40 $\mu\text{m}$ (649 $\text{cm}^{-1}$ to 1136 $\text{cm}^{-1}$ ).
Spectral Response	
Full width at 1/2 peak	$\Delta\lambda$
Spectral Resolution	$\lambda/\Delta\lambda > 1200$
Spectral Sample	
Spacing	$\Delta\lambda/2$
Sidelobes	> 95 percent of peak at spectral response function within $\pm \Delta\lambda$ from center
Spatial Coverage	$\pm 49.5$ deg from nadir with 1.1 deg diameter FOV
Signal to Noise for Each FOV With a 250-K Scene	< 0.2 K NEDT at $\lambda < 13.6 \mu\text{m}$ < 0.35 K NEDT at $\lambda > 13.6 \mu\text{m}$

---

Table 2. Focal Plane Requirements

---

Configuration	Multiple Linear Arrays
Pixel Size	50 by 100 $\mu\text{m}$
Spectral Resolution Element	100 by 200 $\mu\text{m}$
Dynamic Range	3000
Sample Time	1.25 msec
Total Resolution Element Count	1218
Operating Temperature	60 K
Active Power Dissipation	<200 mW
Detector Outages	<2%
Total Radiation Dose	<18,000 rad (Si)

---

## Figure Captions

- Fig. 1. The AIRS Scan Geometry covers a  $\pm 49.5$  deg wide swath perpendicular to the spacecraft ground track. This pattern is matched to the AMSU scan pattern for optimum cloud clearing.
- Fig. 2. The X-ray View of the AIRS Instrument shows the key mechanical structures and assemblies. The spectrometer is small compared to the volume required to support space radiators and electronics in a configuration consistent with the spacecraft interface constraints.
- Fig. 3. AIRS Multi-Aperture Spectrometer Concept Schematic. The position of the aperture masks determines the location of the arrays in the focal plane.
- Fig. 4. AIRS Spectrometer Optical Schematic. The optical elements will be mounted in a diamond-turned aluminum housing to maximize long-term alignment stability.
- Fig. 5. The entrance pupil slit is spectrally dispersed by the grating. Each entrance slit maps into an array on the AIRS Focal Plane.
- Fig. 6. The AIRS Focal Plane Cryostat Concept uses redundant compressors/displacer pairs to insure 5-yr lifetime. The focal plane, the coldest point on the EOS spacecraft, is housed inside a hermetically sealed dewar to minimize contamination by condensibles in orbit.
- Fig. 7. The predicted AIRS System Sensitivity meets or exceeds the requirements.

SCAN PATH

- ALTITUDE: 705 Km
- SCAN PERIOD: 2.667s
- RES EL: 90
- CONTINUOUS SCAN
- IFOV: 1.1 deg.
- EFFIC: 75%

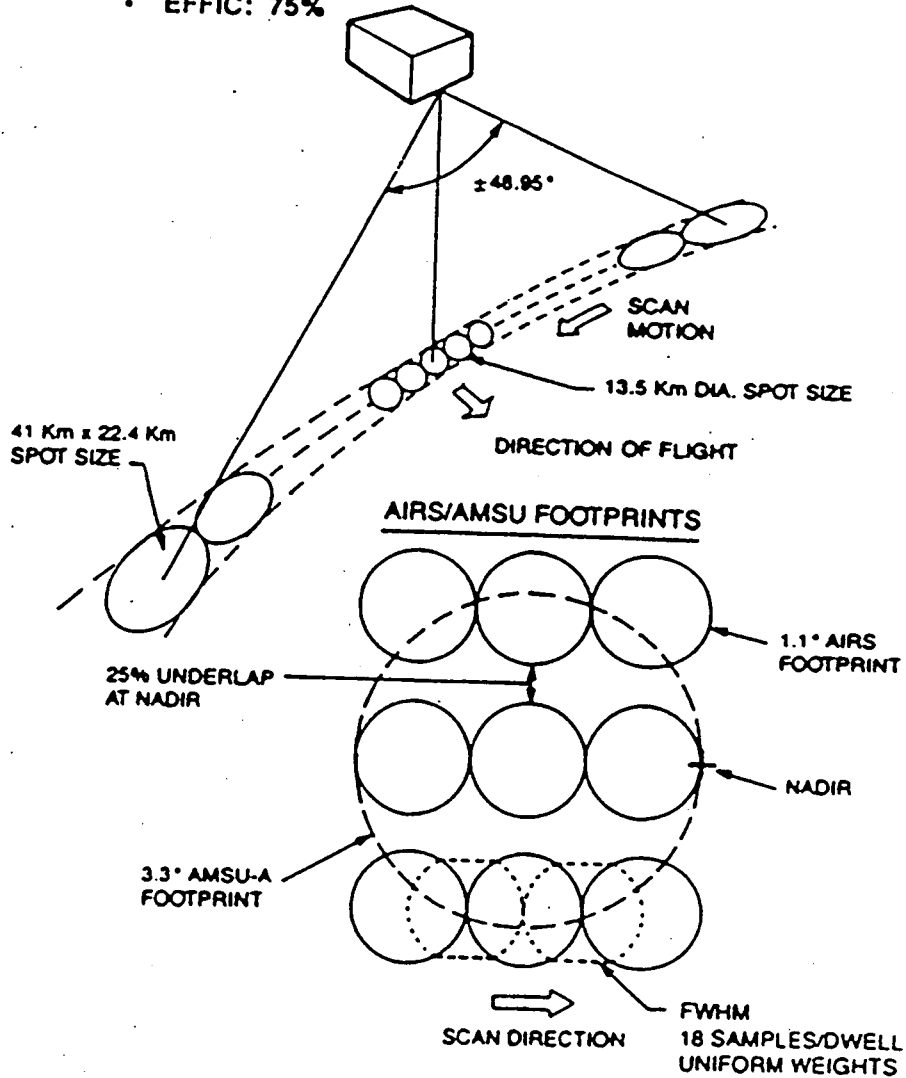


Figure 1. The AIRS Scan Geometry covers a  $\pm 49.5$  degree wide swath perpendicular to the spacecraft ground track.

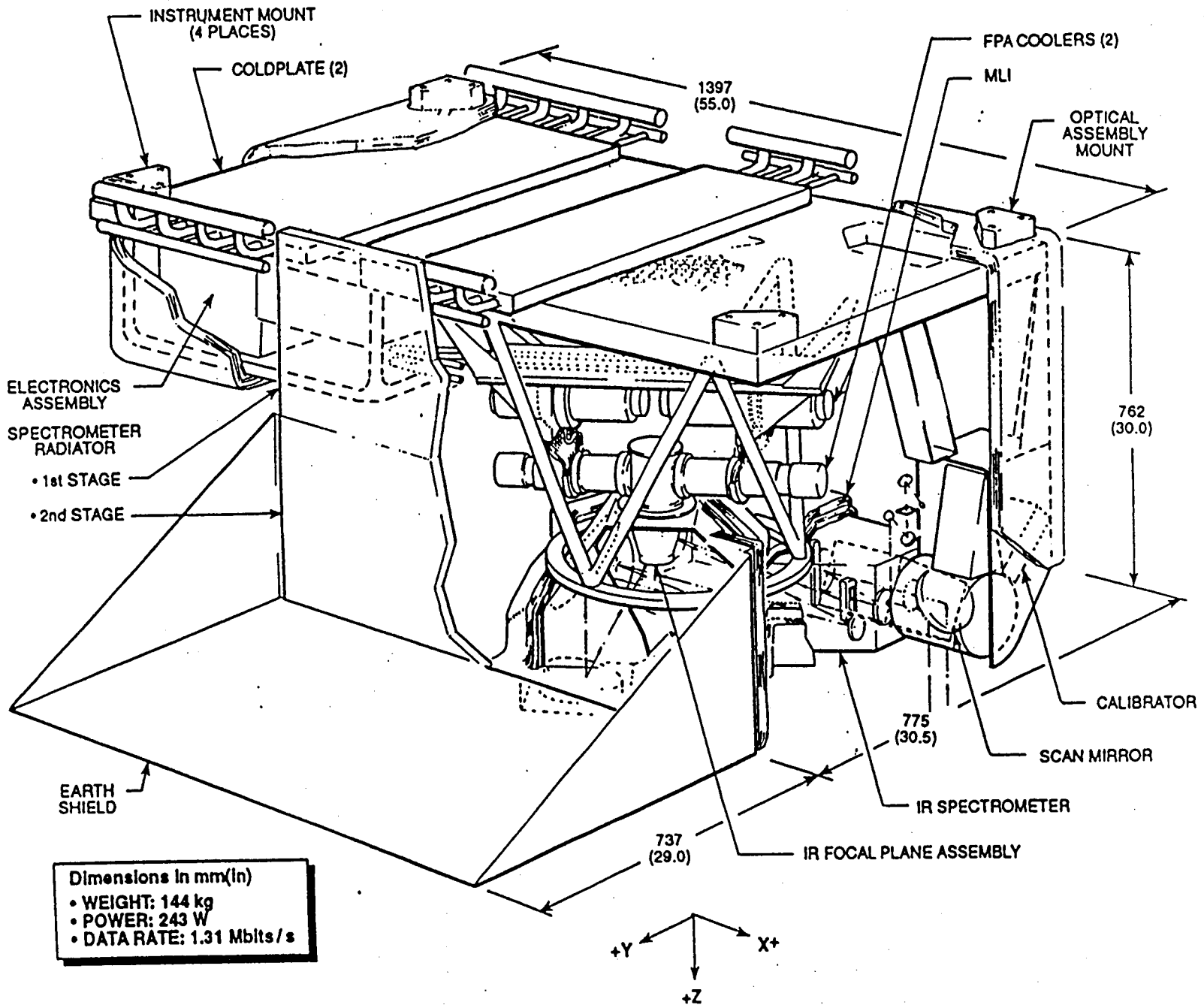


Figure 2. The X-ray View of the AIRS Instrument shows the key mechanical structures and assemblies. The spectrometer is small compared to the volume required to support the spacecraft interface constraints.

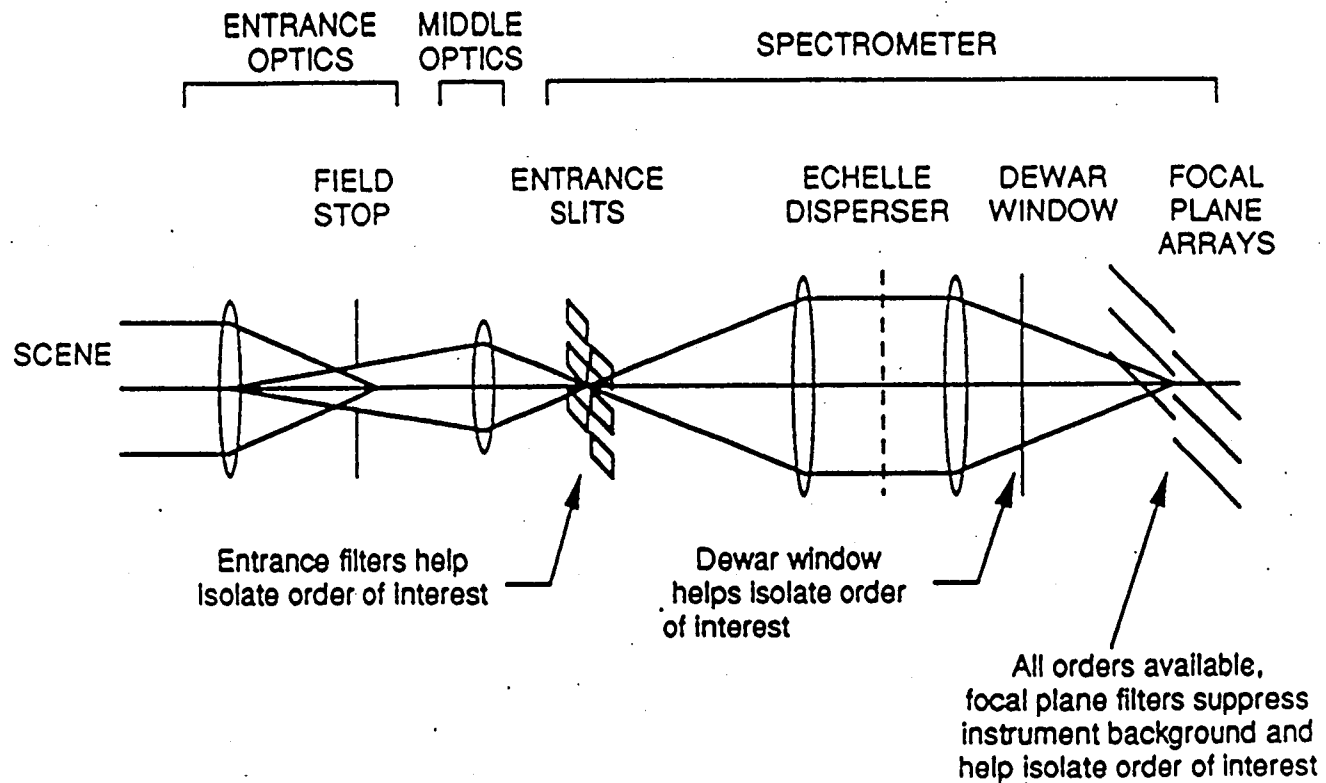


Figure 3. AIRS Multi-Aperture Spectrometer Concept Schematic. The position of the aperture masks determines the location of the arrays in the focal plane.

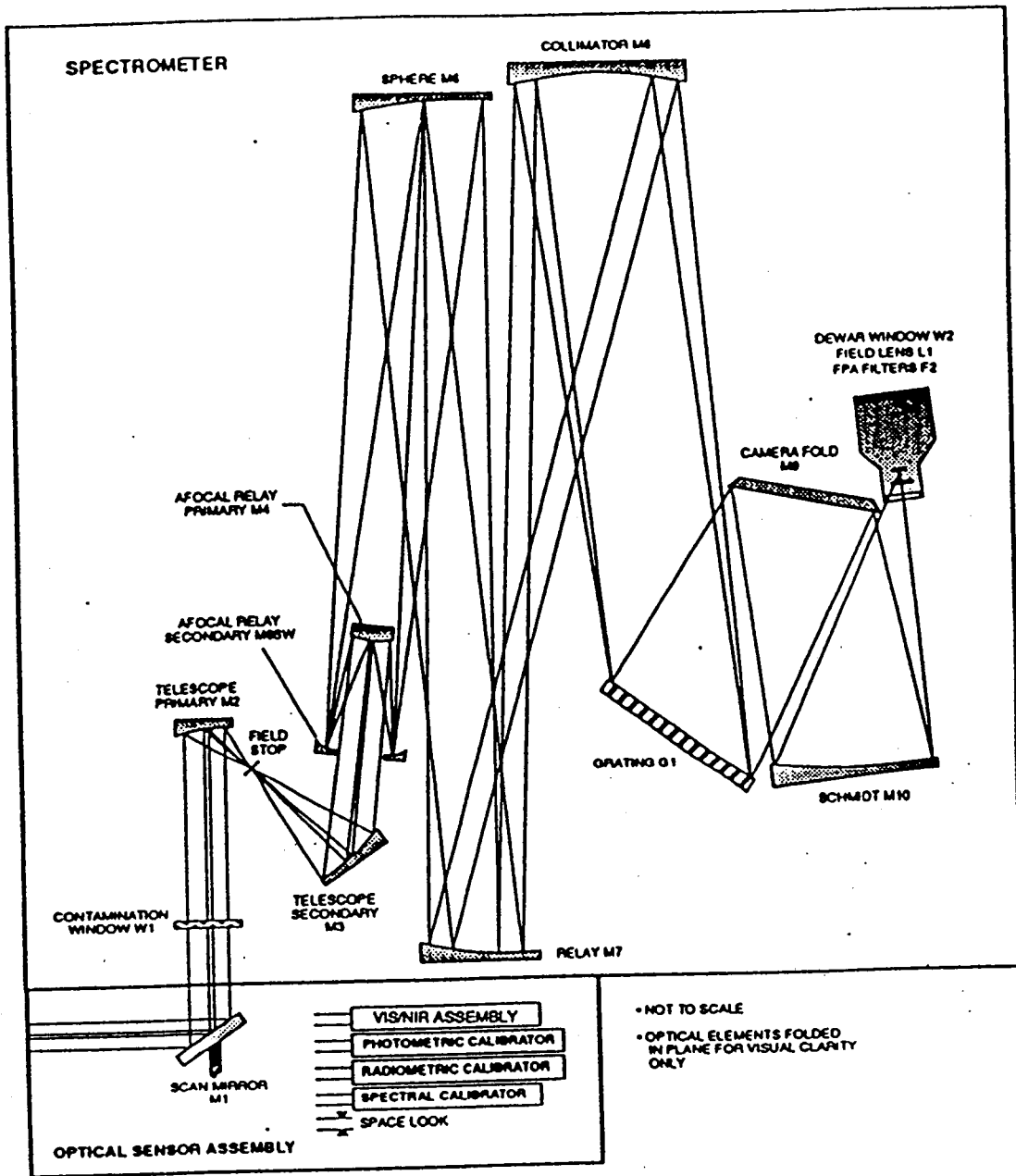
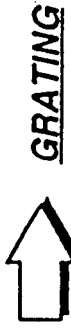


Figure 4. AIRS Spectrometer Optical Schematic. The components will be mounted in diamond turned Aluminum housing.

**ENTRANCE PUPIL SLIT MAP**



**GRATING**



**FOCAL PLANE COLOR MAP**

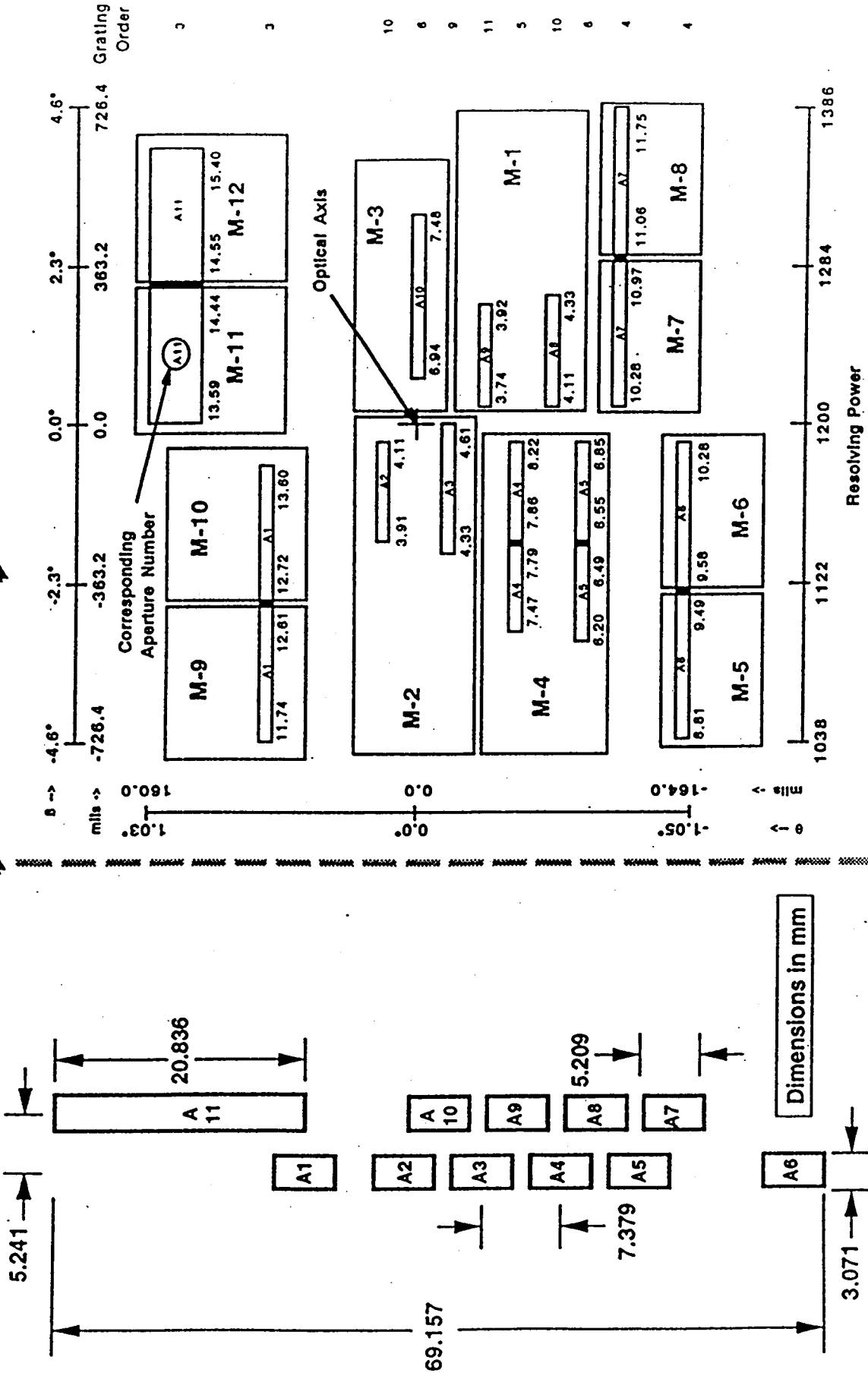


Figure 5. The dispersed entrance pupil slit map becomes the AIRS Focal Plane Map.

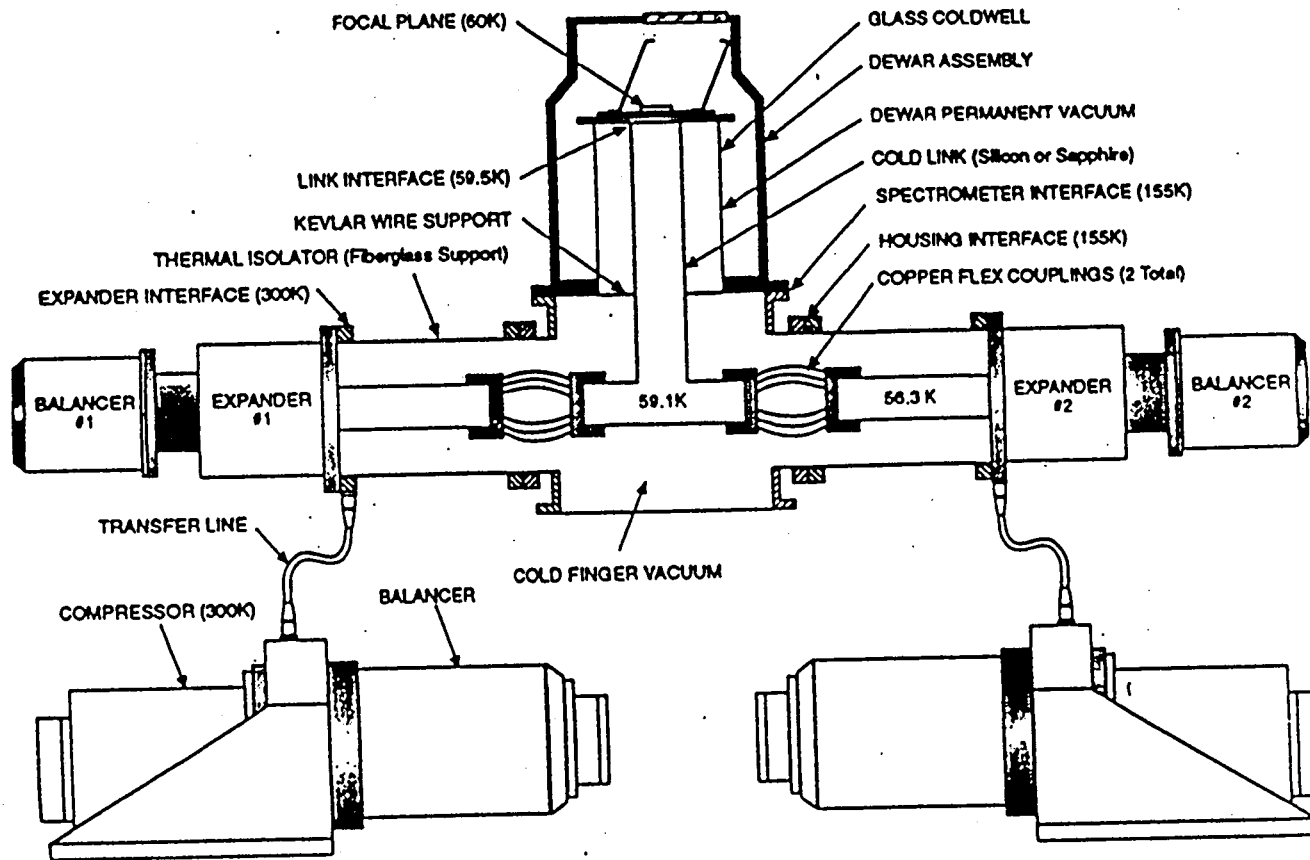


Figure 6. AIRS Focal Plane Cryostat Concept. Two compressors are used to insure five year lifetime. The dewar window permits instrument checkout (but not calibration) outside of a vacuum chamber.

AIRS NE $\Delta$ T - Nominal 250K Scene  
Single FOV Measurement

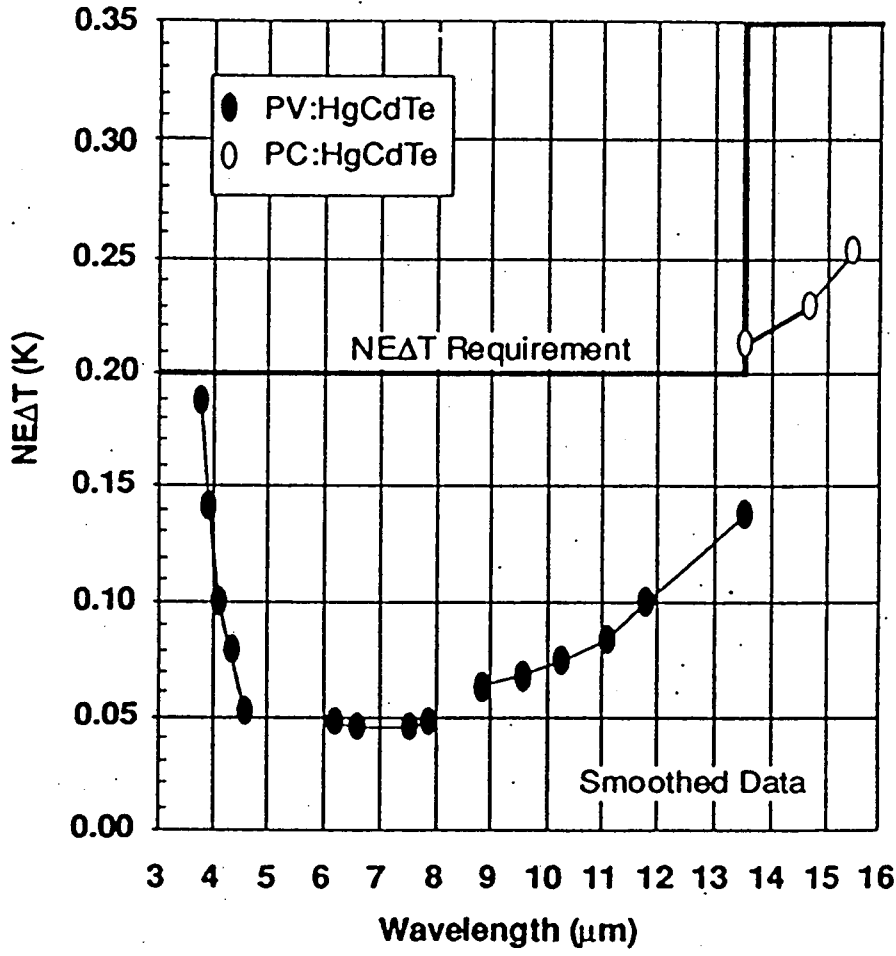


Figure 7. The predicted AIRS System Sensitivity meets or exceeds the requirements.